INTERNATIONAL JOURNAL FOR NUMERICAL METHODS IN FLUIDS
Int. J. Numer. Meth. Fluids 2000; **34**: 145–166

A fast non-Fickian particle-tracking diffusion simulator and the effect of shear on the pollutant diffusion process

Paul S. Addison*[,1], Alberto S. Ndumu and Bo Qu

School of the Built Environment, Napier University, Merchiston Campus, Edinburgh, U.K.

SUMMARY

This paper presents a fast method for the generation of non-Fickian particle paths within a particle-tracking pollutant diffusion model based on a Fourier spectral representation of fractional Brownian motion (fBm), a generalization of ordinary Brownian motion. Correlated diffusive components in a particle-tracking algorithm are modelled using fBm increments that have long-range correlations over numerous spatial and/or temporal scales; hence producing non-Fickian diffusion. A fast algorithm to generate fBm and its increment by using its power spectral density $S(f)$ in a fast Fourier transform algorithm is given. A general equation for the scaling of fBm within a velocity flow field with simple linear shear is presented. An initial numerical study of the nature of fBm shear dispersion has been conducted by incorporating fBm increments into a non-Fickian particle-tracking algorithm. It is shown that the effect of simple (i.e. linear) shear on the diffusion process is to produce enhanced diffusive phenomena with the longitudinal spreading of the plume scaling with exponent $\sim 1 + H$, where H is the Hurst exponent used to describe fBm. Finally, a more complex shear zone at the entrance of a coastal bay model is investigated using both a traditional particle-tracking method and the fBm-based method.

KEY WORDS: fast Fourier transforms; fractal; fractional Brownian motion; non-Fickian diffusion; particle tracking; pollutant; shear dispersion; spectral method

1. INTRODUCTION

Non-Fickian diffusion is frequently observed in pollutant diffusion processes due to the long-range correlations (Lagrangian memory effects) in velocity flow fields. These correlations exist over large spatial scales. Traditional particle-tracking techniques model the diffusion process using uncorrelated random displacements drawn from a Gaussian probability distribution [1–3]. This method leads to the size of the resultant diffusing cloud scaling linearly with the square root of time since release, i.e. Fickian diffusion. In reality, diffusion processes are

* Correspondence to: School of the Built Environment, Napier University, Merchiston Campus, 10 Colinton Road, Edinburgh, EH10 5DT, U.K.
[1] E-mail: p.addison@napier.ac.uk

Received May 1999
Revised September 1999

non-Fickian, with the size of the diffusing cloud scaling non-linearly with time since release due to long-range spatial correlations.

Recently, a new technique has been suggested by the authors [4–7] for the simulation of non-Fickian diffusion within a particle-tracking diffusion model. The technique employs fractional Brownian motion (fBm), a class of random fractal functions [8] opened up by the work of Mandelbrot and Van Ness [9], Mandelbrot and Wallis [10] and Mandelbrot [11] on fractal geometry. fBm processes contain 'memory effects' owing to trends of correlated lags. These correlations appear over all scales and allow for non-Fickian power-laws to be exhibited by particle plumes within particle-tracking diffusion models in which fBm increments model the diffusive steps [6,7]. fBms comprise a generalized family of random fractal functions characterized by an index H, the Hurst exponent [12], which is related to the autocorrelation properties of the function. For $0 < H < \frac{1}{2}$, there is negative correlation, for $\frac{1}{2} < H < 1$, the correlation is positive, and $H = \frac{1}{2}$ is the special case of Brownian motion with zero correlation (see Section 2). For a review of traditional particle-tracking models using uncorrelated diffusive steps and its shortcomings, fBm and other fractal processes and their application in science and engineering, the reader is referred to References [6,7] and the references cited therein.

The layout of this paper is as follows. In Section 2, a review of one-dimensional fBm and its use in simulating non-Fickian diffusion within a particle-tracking diffusion model is outlined. Also in this section, the computational effort associated with integrating the fBm function with finite memory is described. Section 3 provides a spectral representation of the increments of one-dimensional fBm, which is less complicated than the spectral representation of fBm itself. Owing to the stationarity of the fBm increments (fBm comprises a non-stationary process), it is much more accurate, efficient and easier to simulate the increments; then fBm with index H is obtained by summation of its increments with the same index. Recognizing the spectral representation of fBm increments as the sum of sine and cosine functions, it is shown how fBm can be simulated using fast Fourier transform (FFT) techniques. Using FFTs, significant savings can be yielded in terms of the computational effort expended in integrating the fBm function at each time step over a finite memory. Section 4 presents and discusses example applications of the model to simulate pollutant diffusion within numerically generated velocity fields. In this section both a simple, linear shear profile and a more complex non-linear spatially varying velocity field are investigated. Finally, some concluding remarks are made in Section 5.

2. THE fBm PARTICLE-TRACKING DIFFUSION MODEL

fBm, $B_H(t)$, introduced by Mandelbrot and Van Ness [9] is a continuous random function with zero mean increments and variances, which scale as $\sim t^{2H}$, where t is the time variable and H is the Hurst exponent. fBm is expressed as

$$B_H(t) = \frac{1}{\Gamma(H+\frac{1}{2})} \int_{-\infty}^{t} (t-s)^{H-1/2} \, \mathrm{d}W(s) \tag{1}$$

where $dW(s)$ represents increments of a standard Wiener process, and $\Gamma(H+\frac{1}{2})$ is a gamma function introduced to insure that the fractional integral becomes an ordinary integral when $H-\frac{1}{2}$ is an integer. fBm is a biased random process, where the bias comes about by simply weighting each independent increment $dW(s)$ by a factor of $(t-s)^{H-1/2}$. Therefore, within a sub-interval, the function $B_H(t)$, at any time t, may be found by adding up the increments up to a time t, given the initial value $B_H(0)$ at the beginning of the sub-interval, which is similar to the simulation of a random walk by the summation of uncorrelated increments taken from a Gaussian distribution. Within a particular fBm sub-interval, past increments may be correlated with future increments in the following way: given the initial value of $B_H(0)$ at $t=0$, the autocovariance of past increments, $\Delta B_1 = B_H(t) - B_H(0)$ and $\Delta B_2 = B_H(2t) - B_H(t)$ at times t and $2t$ respectively, is $E\{[\Delta B_1 - E(\Delta B_1)][\Delta B_2 - E(\Delta B_2)]\}$. If we then divide by the variance of ΔB_H, the correlation function of fBm increments may be written as

$$C(t) = 2^{2H-1} - 1 \tag{2}$$

From Equation (2) we see that the correlation depends only on the exponent H and not on the time variable t. Within a sub-interval, the function $C(t)$ measures the correlation over period t, where t can be of any length—i.e. events in one period may affect events in all subsequent periods. For $H=\frac{1}{2}$, the correlation $C(t)$ vanishes for all t and the process reduces to the special case of ordinary Brownian motion, or random walk, consisting of a series of independent increments. For $H \neq \frac{1}{2}$, then $C(t) \neq 0$, *independent* of t, and the correlation structure of the process shows a slow decay. This leads to what is called persistent ($H > \frac{1}{2}$) and antipersistent ($H < \frac{1}{2}$) sub-intervals in the fBm process [4]. Insight into the nature of fBm may be obtained by implementing such a process by computer simulation to generate the one-dimensional process. The fBm integral expression given in Equation (1) is divergent as $s \to -\infty$, which makes the generation of fBm difficult. In order to generate the fBm process, Mandelbrot and Van Ness [9] derived the following expression for $B_H(t)$, given the value of $B_H(t=0)$:

$$B_H(t) - B_H(t=0) = \frac{1}{\Gamma(H+\frac{1}{2})} \int_{-\infty}^{t} K(t-s)\, dW(s) \tag{3}$$

Here the simple power-law kernel in Equation (1), $(t-s)^{H-1/2}$, is replaced by the modified kernel

$$K(t-s) = \begin{cases} \{(t-s)^{H-1/2}\}, & 0 \leq s \leq t \\ \{(t-s)^{H-1/2} - (-s)^{H-1/2}\}, & s < 0 \end{cases}$$

This expression vanishes quickly enough as $s \to -\infty$ to make the expression properly define the random function $B_H(t)$. In Addison *et al.* [6,7], a discretized approximation to the fBm integral of Equation (3) using a finite limited temporal memory $M\Delta t$ was given, where $M\Delta t$ is much larger than the time scale, $N\Delta t$, of the problem under consideration. In practical terms, it means that to generate N fBm steps, $B_H(t)$, we require $N+M$ random steps taken from a Gaussian or simpler probability distribution [8]. The larger the memory M used, the

better is the resulting approximation to the fBm. In practice, M requires to be at least ten times larger than N for a good approximation [8]. There is an obvious computational cost involved in using the discretized expression given in Addison *et al.* [6] as each time step in the fBm function in each spatial direction requires the summation of M previous steps. This compared with simply adding on a single Gaussian random variable of known standard deviation in the Fickian (Brownian) particle-tracking model. To overcome the computational burden expended in integrating the fBm function with finite memory, herein we simulate non-Fickian diffusive particle paths using a much faster method to generate fBm increments using its spectral properties. The discrete computation of fBm increments of length N requires N^2 operations. In the next section we show that by expanding the generating function of fBm increments in terms of sine and cosine functions, increments of fBm can be calculated using a fast Fourier transform (FFT) algorithm, thereby achieving considerable savings on computational time expended in integrating the fBm function. With an FFT algorithm, the evaluation of fBm increments requires $N \log_2 N$ operations to generate a series of N points.

3. SPECTRAL GENERATION OF fBm INCREMENTS WITH LONG-RANGE CORRELATIONS USING FFT

A variety of methods has been suggested for the generation of fBm [13–16], however, these methods are either inaccurate, produce inefficient approximations of fBm or are computationally very time consuming [14,17,32]. The Fourier filtering method is one such method and is based on the spectral property of fBm. Its uses the Fourier transform (FT) to generate a process that has the spectral density $S(f) \propto f^{(2H+1)}$. However, as criticized by Yin [17], the power-law property of the spectral density is derived by time averaging and is therefore an approximation because fBm is non-stationary and does not possess a time-independent spectrum. Instead, Yin [17] proposes an accurate and efficient simulation algorithm for one- and also multi-dimensional fBm based on the spectral representation of fBm *increments*. As pointed out, fBm is non-stationary while its increment is stationary. All previous methods of generating fBm deal directly with fBm itself, which makes the simulations complicated and inaccurate because of fBm's non-stationarity. Yin [17] suggests generating fBm increments, known as fractional Gaussian noises (fGn), which comprise a discrete stationary process with power-law correlations at various spatial and/or temporal scales; then fBm with index H is obtained by summation of its increments. The fBm increment $R_H(t)$ is defined as

$$R_H(t) = B_H(t + \Delta t) - B_H(t) \tag{4}$$

When $H = \frac{1}{2}$, $R_H(t)$ is equivalent to $\mathrm{d}W(s)$ given in Equation (3) (i.e. uncorrelated Brownian increments). Discrete fBm is obtained from Equation (4) as

$$B_H(t_i) = \sum_{k}^{i} [B_H(t_k) - B_H(t_{k-1})] = \sum_{k}^{i} R_H(t_{k-1}) \tag{5}$$

That is, to simulate fBm $B_H(t_i)$ at time t_i with index H, the noises $R_H(t_k)$ $(k = 1, \ldots, i)$ are first simulated, then fBm with the same index is obtained using Equation (5). Equation (5) reduces to the expression used to simulate random walk or regular Brownian motion when $H = \frac{1}{2}$, $R_H(t_i)$ represents the diffusive component per time step Δt, which is added to an advection term in a particle-tracking algorithm [7] in which the random displacements have long-range correlations. Using $R_H(t_i)$, we can model non-Fickian diffusion with non-linear scaling of the diffusion coefficient for various values of the Hurst exponent H. Depending on the exponent H, the function $R_H(t_i)$ can model superdiffusion $(H > \frac{1}{2})$, where the variance of the diffusing cloud increases faster than linearly with time or sub-diffusion $(H < \frac{1}{2})$ in which the variance increases slower than linearly [8]. $H = \frac{1}{2}$ models regular Brownian (Fickian) diffusion. The definition of the autocovariance function $C(r)$ of a fGn process is given as

$$\begin{aligned} C(r) &= \operatorname{cov}\{R_H(t),\ R_H(t+r)\} = E\{[R_H(t) - E(R_H(t))][R_H(t+r) - E(R_H(t+r))]\} \\ &= E\{R_H(t+r)R_H(t)\} - E^2\{R_H(t)\} \end{aligned} \tag{6}$$

Derivation of the autocovariance function of fGn $C(r)$ in terms of its variogram $\gamma(r)$ gives

$$\gamma(r) = E\{R(t)^2\} - E^2\{R(t)\} - C(r) \tag{7}$$

Using this relation and the Weiner–Khintchine theorem, then the power spectral density $S(f)$ of one-dimensional fGn is given as [17–19]

$$S(f) = \sum_{r=-\infty}^{\infty} C(r)\cos(2\pi r f) \tag{8}$$

where f denotes the frequency and $r = 0, \pm 1, \pm 2$; $-\frac{1}{2} \le f \le \frac{1}{2}$. The power spectral density and autocovariance functions of fGn represent FT pairs. Given the power spectral density function $S(f)$, we derive the following expression for $R_H(t)$ using the modified spectral method of Shinozuka and Jan [23]. $R_H(t)$ is given as

$$R_H(t) = \sqrt{2} \sum_{k=-N/2}^{N/2-1} [S(f_k)\Delta f]^{1/2} \cos(2\pi f_k t + \phi_k) \tag{9}$$

where $t = 0, 1, 2, \ldots, N$; $S(f)$ is the spectral density function given in Equation (8); N is the total number of samplings in f; $\Delta f = 1/N$ is the interval of sampling; $f_k = k\Delta f$ are the values of f sampled; and ϕ_k are independent random angles uniformly distributed in $[0, 2\pi]$. Expanding the cosine function in Equation (9) for the increments of fBm in terms of sines and cosines, we obtain the following expression for $R_H(t)$:

$$R_H(t) = \sqrt{2/N} \sum_{k=-N/2}^{N/2-1} [S(k/N)]^{1/2} \left[\cos(\phi_k) \cos\left(\frac{2\pi k t}{N}\right) - \sin(\phi_k) \sin\left(\frac{2\pi k t}{N}\right) \right] \tag{10}$$

where $t = 0, 1, \ldots, N-1$. Equation (10) represents the real part of a more general complex random process $X(t) = R_H(t) + \mathrm{i}\,Y(t)$. A complex FT algorithm can, therefore, be used to construct the complex process $X(t)$, from which the real-valued process $R_H(t)$ can be extracted. Computation of $R_H(t)$ using FTs can be demonstrated as follows: take a general complex number $u_k = \sqrt{S}\cos(\phi_k) + \mathrm{i}\sqrt{S}\sin(\phi_k)$, where $\sqrt{S}$ is a constant and k varies from $-N/2$ to $N/2-1$. The discrete FT of $u_k$is given by

$$T_n = \sqrt{2/N} \sum_{k=-N/2}^{N/2-1} u_k \exp\left(\frac{2\pi \mathrm{i} kn}{N}\right) \tag{11}$$

where $n = 0, \ldots, N-1$. (Note that $\sqrt{2/N}$ is equal to $1/\sqrt{\pi}$ when 2π is the total range and $\frac{1}{2}\pi$ represents the sampling interval; here N is the total number of samplings.) The discrete FT maps N complex numbers (the u_ks) into N complex numbers (the T_ns). Equation (11) can also be written as follows:

$$\begin{aligned} T_n &= \sqrt{2/N} \sum_{k=-N/2}^{N/2-1} \sqrt{S}[\cos(\phi_k) + \mathrm{i}\,\sin(\phi_k)]\cdot\exp\left(\frac{2\pi \mathrm{i} kn}{N}\right) \\ &= \sqrt{2/N} \sum_{k=-N/2}^{N/2-1} \sqrt{S}\exp(\mathrm{i}\phi_k)\cdot\exp\left(\frac{2\pi \mathrm{i} kn}{N}\right) = \sqrt{2/N} \sum_{k=-N/2}^{N/2-1} \sqrt{S}\exp\left(\frac{2\pi \mathrm{i} kn}{N} + \mathrm{i}\phi_k\right) \end{aligned} \tag{12}$$

It is evident that Equation (12) can be calculated using a complex FFT algorithm [20,21] if one inputs $\sqrt{S}\cos(\phi_k)$ as the real part and $\sqrt{S}\sin(\phi_k)$ as the imaginary part of complex data into a complex FFT algorithm. The real part of Equation (12) (the output of the discrete FT) is given by the following equation:

$$\mathrm{real}(T_n) = \sqrt{2/N} \sum_{k=-N/2}^{N/2-1} \sqrt{S}\cos\left(\frac{2\pi kn}{N} + \phi_k\right) \tag{13}$$

Expanding the cosine function of the right-hand side of Equation (13) we obtain

$$\mathrm{real}(T_n) = \sqrt{2/N} \sum_{k=-N/2}^{N/2-1} \sqrt{S}\left[\cos(\phi_k)\cos\left(\frac{2\pi kn}{N}\right) - \sin(\phi_k)\sin\left(\frac{2\pi kn}{N}\right)\right] \tag{14}$$

By making the analogy $\mathrm{real}(T_n) = \mathrm{real}(X(t))$ we observed that $\mathrm{real}(T_n)$ and $R_H(t)$ are identical (where $\sqrt{S} \equiv [S(f_k)\Delta f]^{1/2}$); therefore, if one inputs $[S(f_k)\Delta f]^{1/2}\cos(\phi_k)$ as the real part and $[S(f_k)\Delta f]^{1/2}\sin\phi_k$ as the imaginary part of input complex data, then the real part of output complex data is $R_H(t)$. Press *et al.* [22] provides an FFT algorithm to calculate the discrete FT of N sample points h_k, where k varies from 0 to $N-1$. In Press *et al.* [22], the discrete FT of h_k is given as

$$T_n = \sqrt{2/N} \sum_{k=0}^{N-1} h_k \exp\left(\frac{2\pi \mathrm{i} kn}{N}\right) \tag{15}$$

where $k = 0, \ldots, N-1$. Equation (15) is for sample data points varying from $k = -N/2$ to $N/2-1$. Therefore, to use the algorithm given in Press *et al.* [22], we let $m = k + N/2$, then Equation (15) can be rewritten as

$$T_n = \sqrt{2/N} \sum_{m=0}^{N-1} u_{(m-N/2)} \exp\left(\frac{2\pi \mathrm{i}(m-N/2)}{N}\right) \tag{16}$$

where $n = 0, \ldots, N-1$. Substituting k for m in Equation (16) we obtain

$$\begin{aligned} T_n &= \sqrt{2/N} \sum_{k=0}^{N-1} u_{(k-N/2)} \exp\left(\frac{2\pi \mathrm{i}kn}{N}\right) \exp(\mathrm{i}\pi n) \\ &= \sqrt{2/N} \sum_{k=0}^{N-1} u_{(k-N/2)} \exp\left(\frac{2\pi \mathrm{i}kn}{N}\right)[\cos(\pi n) + \mathrm{i}\sin(\pi n)] \\ &= \sqrt{2/N} \sum_{k=0}^{N-1} u_{(k-N/2)} \exp\left(\frac{2\pi \mathrm{i}kn}{N}\right)(-1)^n = (-1)^n \sqrt{2/N} \sum_{k=0}^{N-1} u_{(k-N/2)} \exp\left(\frac{2\pi \mathrm{i}kn}{N}\right) \end{aligned} \tag{17}$$

From Equation (11)

$$T_n = \sqrt{2/N} \sum_{k=-N/2}^{N/2-1} u_k \exp\left(\frac{2\pi \mathrm{i}kn}{N}\right) \tag{18}$$

or for the computation using the FFT algorithm in Press *et al.* [22], from Equation (17)

$$T_n = (-1)^n \sqrt{2/N} \sum_{k=0}^{N-1} u_{(k-N/2)} \exp\left(\frac{2\pi \mathrm{i}kn}{N}\right) \tag{19}$$

The mapping of $k = -N/2$ to $N/2$ into $k = 0$ to $N-1$ for the spectral density function $S(f_k)$ is therefore given by

$$\sum_{k=-N/2}^{N/2-1} [S(f_k)\Delta f]^{1/2} \equiv \sum_{k=0}^{N-1} [S(f_{k-N/2})\Delta f]^{1/2} \tag{20}$$

Therefore, the algorithm given in Press *et al.* [22] can be used to calculate the fGn function $R_H(t)$ given in Equation (9) by using the power spectral density function in the range $-\frac{1}{2} \le f_k \le \frac{1}{2}$ computed in Equation (8). In this way the fGn components of fBm can be generated and summed to produce fBm through Equation (5). The FFT method presented here is a much faster, more accurate and more efficient method of fBm generation than the one previously proposed by the authors [6,7]. Figure 1 shows the theoretical autocovariance function of fGn computed using the definition given in Equation (6) and the simulated autocovariance for fGn computed using the FFT method for $H = 0.35$ and 0.85. The simulated autocovariance is calculated using the average of 100 independent fGn realizations. It is observed that for a large enough sample of realizations, the autocovariance structure of the

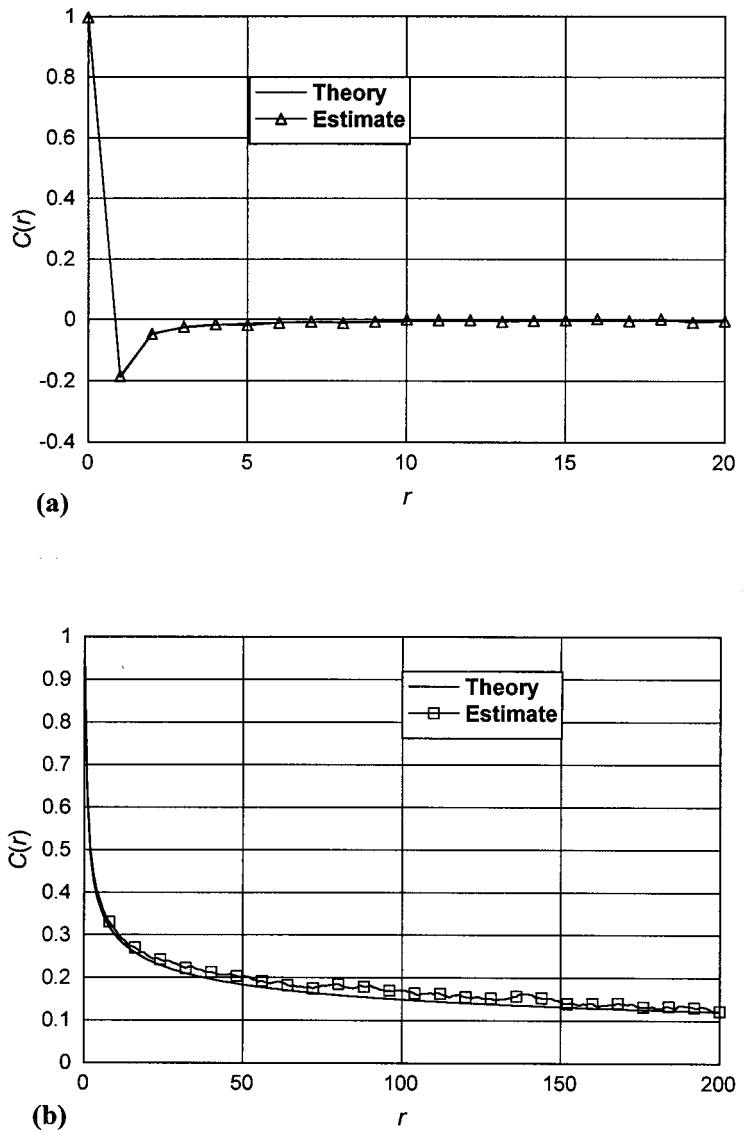

Figure 1. Theoretical autocovariance of fGn and simulated autocovariance calculated using an average of 100 fGn realizations: (a) $H = 0.35$ and (b) $H = 0.85$.

simulated process matches the desired autocovariance structure very closely. In the next section, the fBm increments are incorporated into a particle-tracking pollutant diffusion model to investigate shear diffusion within the coastal zone.

4. fBm DIFFUSION AND SHEAR DISPERSION

It was shown in previous work by the authors [6,7] that by using multiple realizations of fBm within a particle-tracking model, non-Fickian diffusion may be generated in which the standard deviation, σ, of the diffusing particle cloud scales non-linearly with time in a general equation, given as

$$\sigma = (2D_f t)^H \tag{21}$$

where D_f is a non-Fickian (fractal) diffusion coefficient, t is the time since release and H is the Hurst exponent. (See Appendix A for an alternative definition.) Using an fBm particle-tracking model, therefore, allows flexibility in the exponential diffusive scaling of the particle-tracking model [4–8], achieved by simply varying the value of the Hurst exponent, which determines the correlation of the fBm function. The following sub-sections consider the nature of shear dispersion within an fBm particle-tracking model. (fBm dispersion within a constant velocity field is given in Addison *et al.* [4].)

4.1. Simple shear dispersion: linear velocity profile

The rapid spreading of diffusing clouds within regions of marked velocity gradients is a well-documented phenomenon known as shear dispersion. It accounts for much of the rapid spreading of pollutants within the river, estuarine and coastal environments. Much investigative work of a theoretical and numerical nature has concentrated on the dispersion of point sources in simple shear flows [24], which consists of a linear variation in the velocity profile described by

$$V(y) = \alpha x \tag{22}$$

where α is the shear gradient. An example of a simple (i.e. linear) shear flow is illustrated in Figure 2 for a shear gradient $\alpha = 0.0003$. If a point source of contaminant is released within such a shear flow, then, for a Fickian cloud, we get the well-known result [24] for the rate of spreading orthogonal to the flow

$$\sigma_x^2 = 2Dt \tag{23}$$

and along the direction of the flow given by

$$\sigma_y^2 = 2Dt + \frac{2}{3}\alpha^2 D t^3 \tag{24}$$

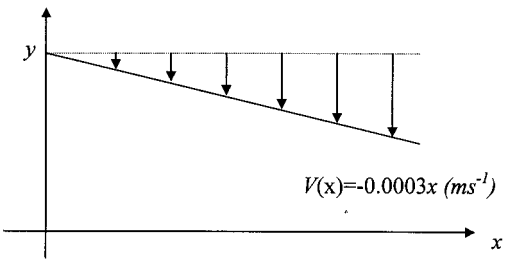

Figure 2. Velocity profile for simple shear.

For large times, Equation (24) reduces to

$$\sigma_y^2 = \frac{2}{3}\alpha^2 D t^3 \tag{25}$$

Figure 3 contains the results of a pollutant shear dispersion simulation using the shear flow in Figure 2. A traditional particle-tracking method (i.e. $H = \frac{1}{2}$) is used with D, the diffusion

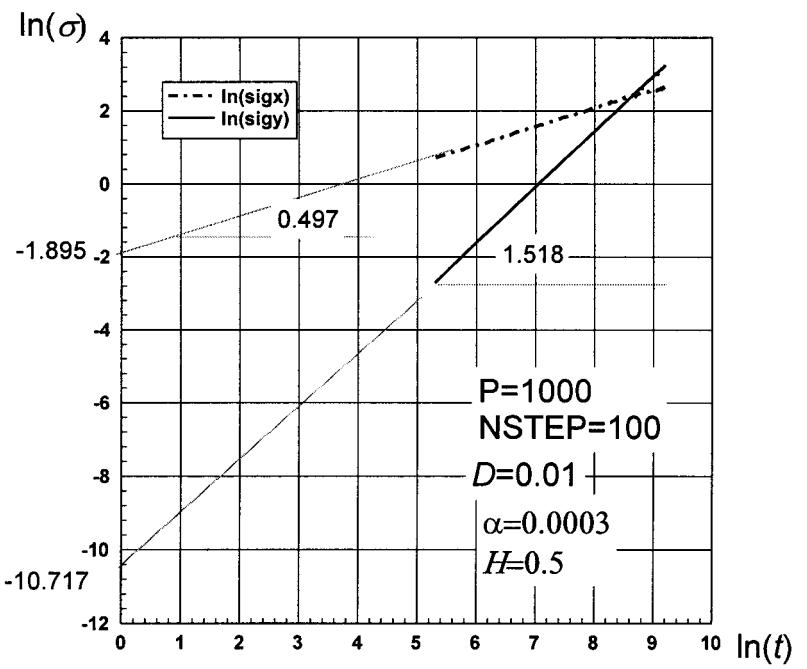

Figure 3. Plot of $\ln(\sigma_x)$ and $\ln(\sigma_y)$ versus $\ln(t)$ for $H = 0.5$, $D = 0.01$, $\Delta t = 10$, 1000 particles, 100 steps. (In the figure, σ_x is denoted sig$x$ and σ_y is denoted sig$y$.)

coefficient, set equal to 0.01 in the x- and y-directions (a typical value used in engineering practice for estuarine flows). In the figure, the natural logarithm of standard deviation of the transverse (σ_x) and longitudinal (σ_y) cloud patch is plotted against $\ln t$. This is done for a simulation consisting of 1000 non-reactive particles to represent the pollutant mass and, even for this low number of particles, the slopes of the plots are very close to the expected theoretical scaling exponents of $\frac{1}{2}$ and $\frac{3}{2}$, from Equations (23) and (25) respectively. Equation (23) and (25) can be generalized to the scaling of fBm within shear flows. Using fBms, the rate of spreading orthogonal to the mean flow direction would now take the form [8]

$$\sigma_x = (2D_f t)^H \tag{26}$$

We hypothesize herein that, since the rate of spreading of the pollutant cloud is a combination of the influence of the linear shear dispersion and exponential (H) fBm diffusion, the spreading along the mean velocity direction can be generalized from Equation (25) as

$$\sigma_y^2 = C\alpha^2(2D_f t)^{2H} t^2 \tag{27}$$

that is

$$\sigma_y = \sqrt{C}\alpha 2^H D_f^H t^{1+H} \tag{28}$$

where C is a constant and D_f is the fractal diffusion coefficient. Equation (28) shows that the effect of simple shear dispersion on the longitudinal dispersion process using fBm is an enhanced diffusive spreading of the particle cloud scaling with time t as $\sim t^{1+H}$. Equations (27) or (28) reduce to Equation (25) when $H = \frac{1}{2}$, with $C = \frac{1}{3}$ and $D_f = D$, the normal Fickian diffusion coefficient. Taking the natural logarithms of both sides of Equation (28) then

$$\ln(\sigma_y) = \ln(\sqrt{C}\alpha 2^H D_f^H) + (1+H)\ln(t) \tag{29}$$

Substituting the values of $\alpha = 0.0003$ and $D_f = 0.01$ into Equation (29) we obtain

$$\ln(\sigma_y) = \ln(0.0003\sqrt{C}) + H\ln(0.02) + (1+H)\ln(t) \tag{30}$$

Thus, a plot of $\ln(\sigma_y)$ against $\ln(t)$ should give a curve of slope $1+H$ and an intercept A_y at

$$A_y = \ln(\sqrt{C}) - 8.1117 - 3.9120H \tag{31}$$

Hence C can be obtained. Figure 4(a)–(d) show the results of four fBm particle-tracking simulations of particle clouds (1000 particles) spreading in shear flows using Hurst exponents of $H = 0.6$, 0.7, 0.8 and 0.9. (We restrict ourselves to superdiffusive Hurst exponents as we know from experimental studies [26–28] that ocean drifter trajectories are superdiffusive in nature.) We see from the plots that orthogonal to the flow σ_x scales as in Equation (26). This behaviour is as expected, as the velocity gradient plays no part in the spreading of the cloud in this direction and hence the patch spreads in this direction as for an fBm particle cloud

(Equation (21)) within a uniform flow field. The standard deviation of the diffusing cloud within the flow field in the longitudinal direction y scales as $\sigma_y \sim t^{1+H}$, as predicted by Equation (28). Table I shows the values of H input to the fBm model together with both the values of H and A_y obtained respectively from the slopes and intercepts of the logarithmic

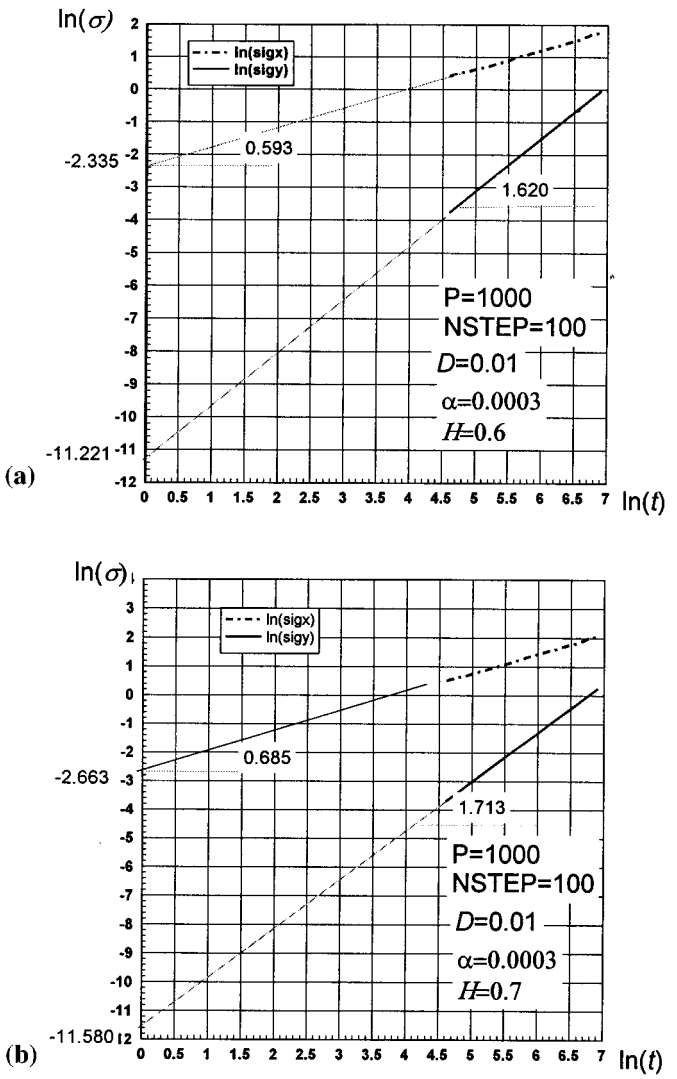

Figure 4. Plots of $\ln(\sigma_x)$ and $\ln(\sigma_y)$ versus $\ln(t)$ for (a) $H = 0.6$, (b) $H = 0.7$, (c) $H = 0.8$, (d) $H = 0.9$, $D = 0.01$, 1000 particles, 100 steps. (In the figure, σ_x is denoted sig$x$ and σ_y is denoted sig$y$.)

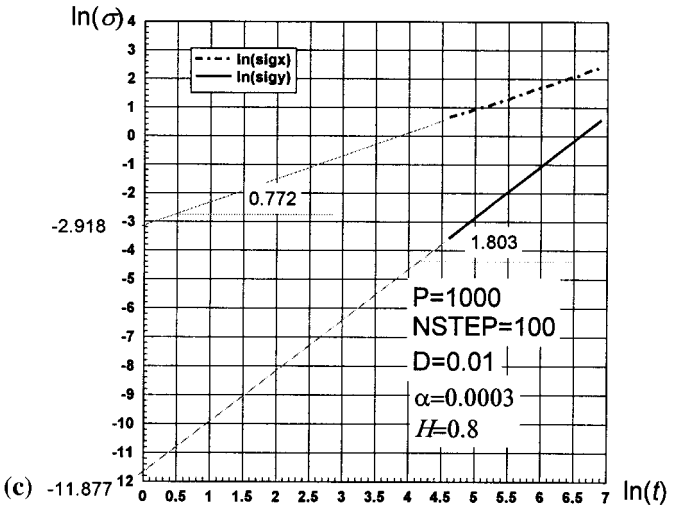

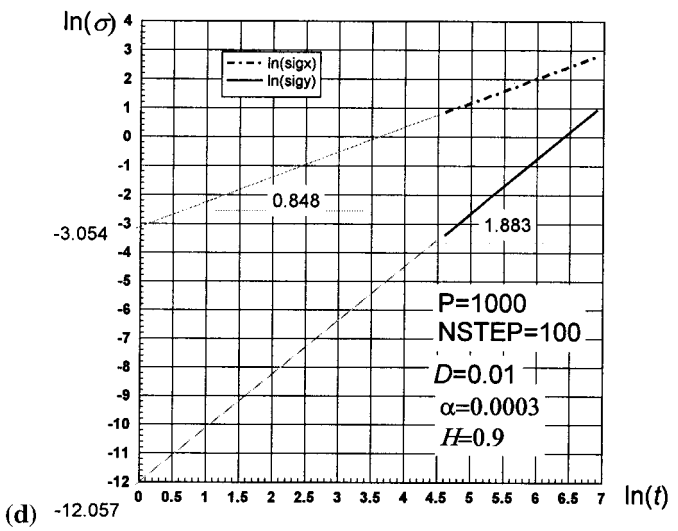

Figure 4 (*Continued*)

plots of σ_y against t given in Figure 4(a)–(d). The realized Hs are used in conjunction with the realized A_y values to obtain a value of C using Equation (31). These are given in the bottom row of Table I. The value of C obtained for each H given in Table I appears to be reasonably close to the theoretical value of $\frac{1}{3}$ for $H = \frac{1}{2}$.

Table I. Input H values to the fBm particle-tracking model together with realized A_y and H values from Figures 3 and 4 and corresponding values of C.

H (input)	0.5	0.6	0.7	0.8	0.9
H (realized from plots)	0.518	0.620	0.713	0.803	0.883
A_y (realized from plots)	−10.717	−11.221	−11.580	−11.877	−12.057
C (using realized H and A_y in Equation (31))	0.314	0.255	0.257	0.287	0.375

4.2. Numerical bay simulation

Here, we investigate pollutant diffusion in a more realistic shear pattern. Figure 5 shows the top surface of a numerically generated velocity vector field of an idealized coastal bay model. (This model is similar to the one used in a previous study by the authors [6], presented in this journal, more information regarding this plot is given in Qu [37].) The main north–south flow generates a recirculation vortex in the bay region. The shear zone region at the bay entrance (between the main flow and the recirculation zone) contains rapidly increasing velocities. Figures 6 and 7 contain the vertical and horizontal velocity profiles respectively across this

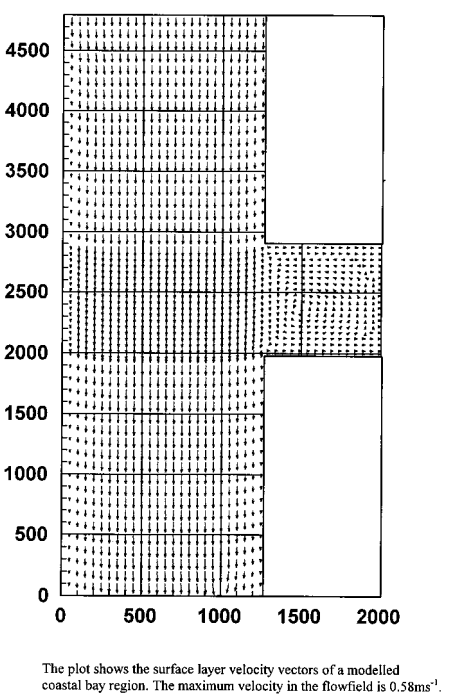

Figure 5. Coastal bay model, velocity vector plot.

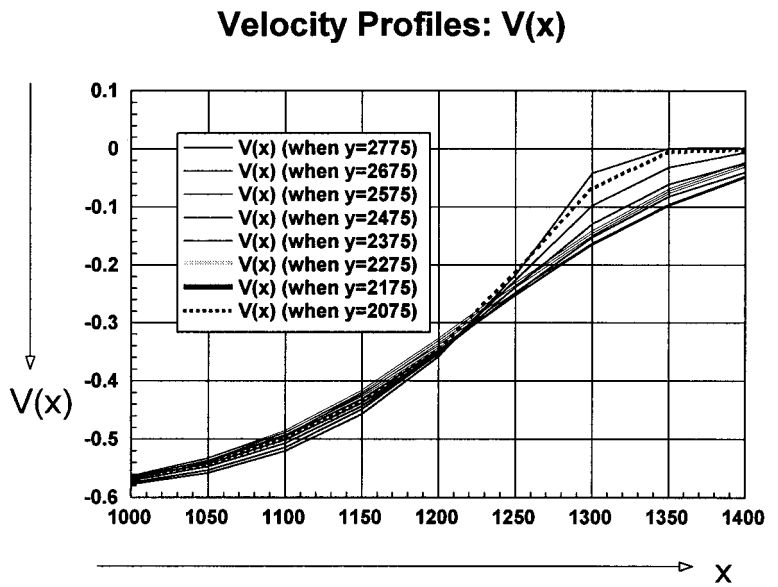

Figure 6. Vertical velocity profiles $V(x)$ at various locations across the bay entrance.

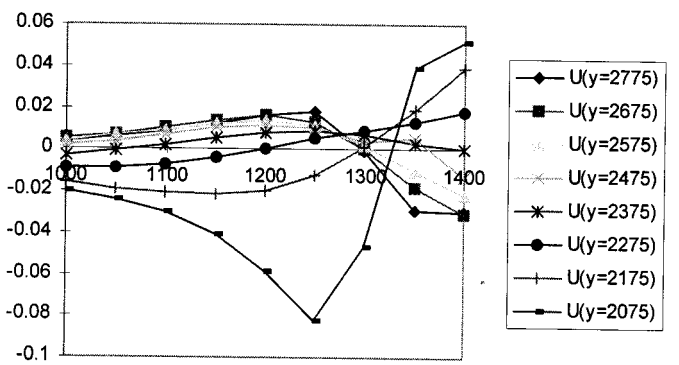

Figure 7. Horizontal velocity profiles $U(x)$ across the bay entrance.

region ($1000 \leq x \leq 1400$ m). The changing directions of the vector field, especially near the top and bottom of the shear region, produce a much more complex shear dispersive process than the simple linear shear considered in the section above. The vertical velocity profiles shown in Figure 6 all show a similar non-linear decrease in the velocity from the main flow (of just under 0.6 m s^{-1} to near zero values). As expected, the profiles nearest the top and bottom of the bay entrance have the highest shear gradients due to the near zero vertical velocity values

close to the bay boundaries. Figure 8 shows plots of $\log(\sigma)$ against $\log(t)$ for spreading particle clouds within the shear zone region released at three different point locations at the top of the bay; namely (1250, 2775), (1300, 2775) and (1350, 2775). The plots contain the spreading in both the x- and y-directions and both for values of H equal to 0.5 (Fickian model—left-hand column) and 0.8 (non-Fickian, fBm model—right-hand column). Both the realized exponent and diffusion coefficients are calculated from the gradient and intercepts of these plots. There is an obvious kink in the top plots in both Figure 8(a) and (b) relating to release point (1250, 2775), where the power-law behaviour of the diffusion changes markedly. The authors believe that this marks a change between the cloud being located solely within the shear layer for earlier times and being spread out across the mean north–south channel flow, shear zone and the recirculation zone at later times. Hence, the gradient over the earlier time is taken as the shear layer power-law. Figure 9 plots the longitudinal and transverse scaling exponents H_x and H_y, computed for the shear dispersion of clouds released at the three points at the top of the shear zone. The values are also given in Table II. The power-law scaling exponents, H_x and H_y, associated with the spreading clouds across the bay shear zone are not simple (i.e. linear) functions of the input Hurst exponent H (as was shown above for the case of simple shear). It is interesting to note, however, that an increase in H_y is associated with a corresponding decrease in H_x. In addition, there is an occurrence of sub-diffusive values of H for the Fickian model. Such sub-diffusive values are sometimes seen in natural estuarine flows.

5. CONCLUDING REMARKS

Over recent years it has become clear that fBm offers a powerful descriptive tool for a variety of spatial and temporal phenomena [30,31]. Herein we have concentrated on its ability to model a certain class of temporal diffusion (defined by Equation (21)) and used it to model non-Fickian diffusive processes in the coastal zone [32]. However, the results presented offer an insight into this class of random fractal function, which has applications elsewhere (see, for example, Reference [30] and the references contained therein).

The equation used to simulate fBm is divergent as time $t \to \infty$, hence most fBm simulation algorithms are either inaccurate and produce inefficient approximations to fBm, or are computationally very time consuming. A fast, accurate and efficient method for the generation of fBm within a particle-tracking diffusion model has been detailed herein. The method uses the spectral characteristics of the derivative of fBm within an FFT algorithm.

An initial numerical study of the nature of shear dispersion for fBm diffusion has been conducted and an equation has been presented for the scaling of fBm shear dispersion. From the numerical results, it is confirmed that, for simple shearing, the standard deviation of the diffusing cloud scales with time t along the flow velocity direction with an exponent equal to $1 + H$, where H is the Hurst exponent. In addition, from our results we speculate that the coefficient C in Equation (27) is a constant over all H equal to $\frac{1}{3}$. However, further numerical work using much larger particle clouds is required to confirm these findings. (In the study presented herein, only 1000 particle clouds were used.)

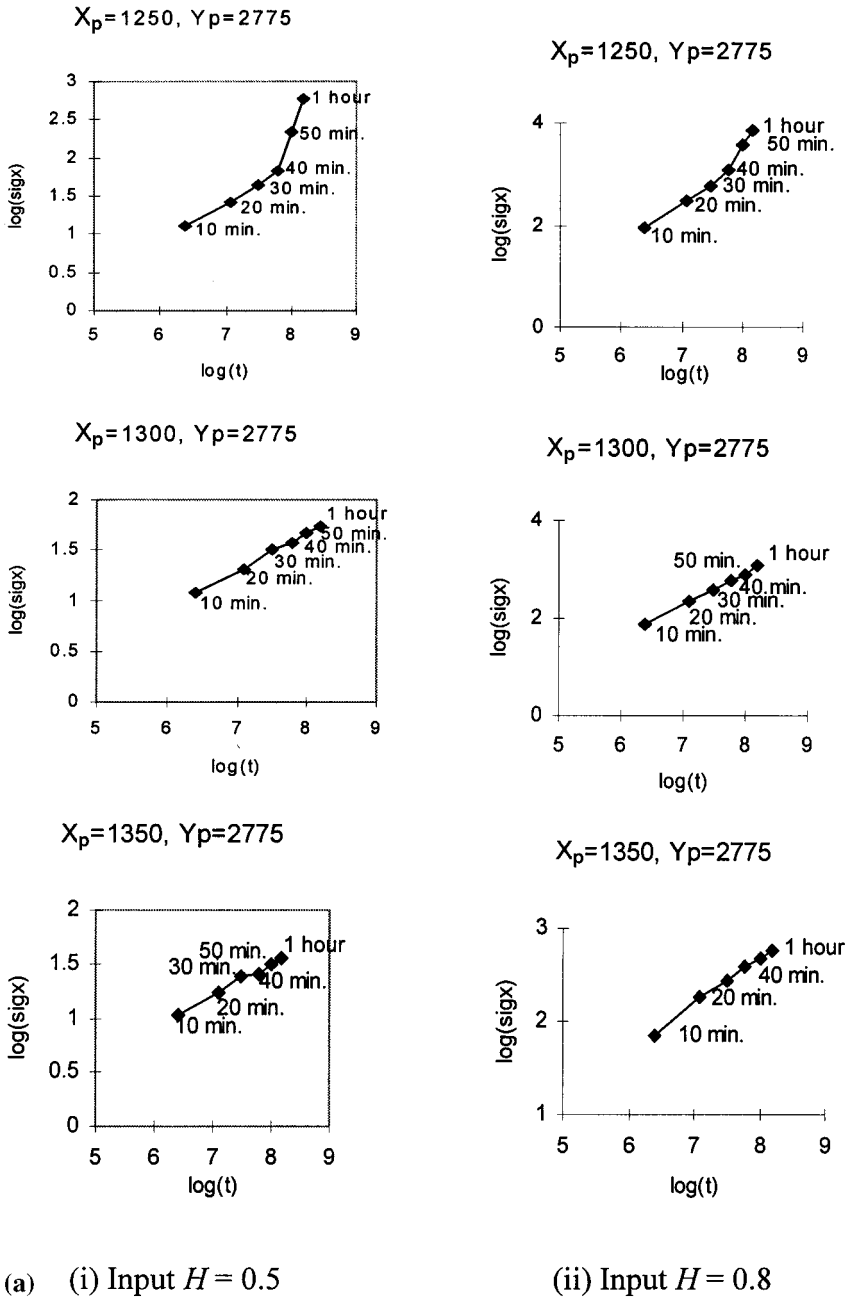

(a) (i) Input $H = 0.5$ (ii) Input $H = 0.8$

Figure 8. Plots of $\log(\sigma_x)$ (a) and $\log(\sigma_y)$ (b) against $\log(t)$ for dispersing particle clouds in the bay shear zone (release points (X_p, Y_p) given in plots.

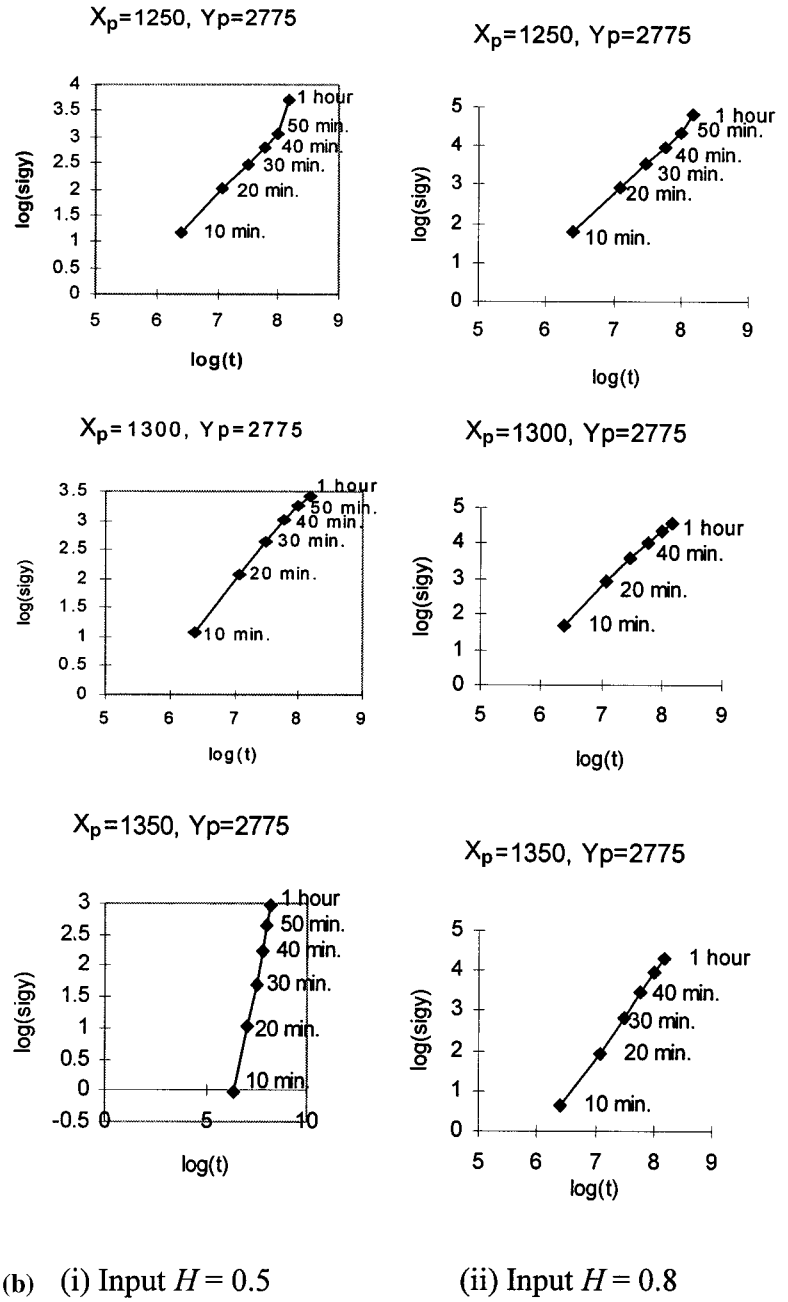

(b) (i) Input $H = 0.5$ (ii) Input $H = 0.8$

Figure 8 (*Continued*)

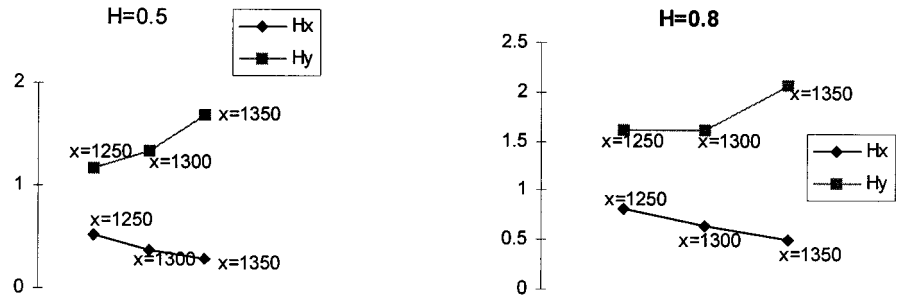

H_x and H_y versus x,
for x = 1250, 1300, 1350, y = 2775.
Input H = 0.5

H_x and H_y versus x
for x = 1250, 1300, 1350, y = 2775.
Input H = 0.8

Figure 9. Realized exponential scalings from the dispersing particle clouds released from various locations at the top of the bay.

Table II. The realized exponential scaling within the shear zone for $H = \frac{1}{2}$ and 0.8 particle clouds released at various x locations and $y = 2775$.

	H_x	H_y
$H = \frac{1}{2}$		
$x = 1250$	0.510	1.173
$x = 1300$	0.370	1.333
$x = 1350$	0.285	1.679
$H = 0.8$		
$x = 1250$	0.813	1.616
$x = 1300$	0.647	1.621
$x = 1350$	0.509	2.065

The nature of shear dispersion across the entrance of a coastal bay model was also investigated. Both Fickian ($H = \frac{1}{2}$) and non-Fickian ($H = 0.8$) particle clouds were released at various locations in this more complex, and realistic, shear region. The results showed a marked sensitivity of the exponential scaling of the resulting shear dispersion to the release point of the cloud. In addition, increases in scaling with the mean flow were coupled with decreases in the orthogonal direction of flow; and in some cases sub-diffusive scaling was found.

Inclusion of fBm within a particle-tracking model leads to more flexibility in the exponential scaling allowed in the simulation. This paper contains details of work in progress by the authors to develop the technique. Further work will include investigation of shear dispersion using much larger particle clouds combined with a theoretical study based on the work of Foister and Van Den Ven [24] using fBm scaling. In addition, work has recently been initiated to use the fBm technique to model datasets obtained from a series of coastal dye studies [25].

This work requires an extension of the fBm particle-tracking method to a full three-dimensional model of the estuarine flow fields. It would also be interesting to extend the particle-tracking model developed by the authors to atmospheric dispersion, especially within the urban environment where alternative models, e.g. Gaussian plume models [33] and their variants [34], find it difficult to cope with the complex topologies and associated flow fields. In such cases Lagrangian stochastic particle-tracking models are beginning to win favour [35,36].

ACKNOWLEDGMENTS

The authors would like to thank Dr G. Pender and Ms Sharon Sloan of Glasgow University for the surface velocity vector field of the coastal bay model used in Section 4.

APPENDIX A. AN EFFECTIVE FOKKER–PLANCK EQUATION FOR fBm DIFFUSION

Recent work [7] by the authors has related fBm diffusion to an effective Fokker–Planck equation [29] to describe non-Fickian or anomalous diffusion given as

$$\frac{\partial P(B_H, t)}{\partial t} = D_e(t) \frac{\partial^2 P(B_H, t)}{\partial B_H^2} \tag{A1}$$

where $D_e(t)$ is the effective diffusion coefficient and $P(B_H, t)$ is the probability density of finding a Brownian particle at displacement B_H at time t. It can be seen that, for a time-independent diffusion coefficient (i.e. for $D_e(t) = D$), Equation (A1) is equivalent to the classical diffusion equation described by ordinary Brownian motion. The diffusive scaling or standard deviation through time t of a diffusive process undergoing fBm non-Fickian diffusion can be defined as

$$\sigma = \sqrt{2D'_f} t^H \tag{A2}$$

where D'_f is a non-Fickian (fractal) diffusion coefficient (of different value to D_f in Equation (21)). Equation (A2) is a generalization of a Fickian or Brownian diffusive scaling. The effective Fokker–Planck equation given in (A1) can be rewritten using Equation (A2) as

$$\frac{\partial P(B_H, t)}{\partial t} = 2HD'_f t^{2H-1} \frac{\partial^2 P(B_H, t)}{\partial B_H^2} \tag{A3}$$

i.e $D_e(t) = 2HD'_f t^{2H-1}$. The solution of Equation (A3) with initial condition $P(B_H, 0) = \delta(B_H)$ (where δ is the Dirac delta function) for an instantaneous point source is

$$P(B_H, t) = \frac{2}{\sqrt{4\pi D'_f t^{2H}}} \exp\left(\frac{-B_H^2}{4D'_f t^{2H}}\right) \tag{A4}$$

which represents the probability density function of finding a Brownian particle at time t at a displacement B_H from its starting point. Equation (A4) is the non-Fickian scaling (i.e. variance not proportional to time) of a Gaussian probability density function through space. Note that Equation (A2) is a slightly different format to Equation (21), although both D_f and D'_f are constants. We used the form of Equation (21) for the discussion in Section 4 as it results in a constant value of $C = \frac{1}{3}$.

REFERENCES

1. Allen CM. Numerical simulation of contaminant dispersion in estuary flows. *Proceedings of the Royal Society, London A* 1992; **381**: 179–192.
2. Allen CM. Particle tracking models for pollutant dispersion. In *Computer Modelling in the Environmental Sciences*, Farmer DG, Rycroft NJ (eds). IMA/Clarendon: Oxford, 1991; 63–75.
3. Hunter JR, Craig PD, Philips HE. On the use of random walk models with spatially variable diffusivity. *Journal of Computational Physics* 1993; **106**: 366–376.
4. Addison PS. A method for modelling dispersion dynamics in coastal waters using fractional Brownian motion. *IAHR Journal of Hydraulic Research* 1996; **34**: 549–561.
5. Addison PS, Qu B. Non-Fickian random walk diffusion models. In *Environmental and Coastal Hydraulics: Protecting the Aquatic Habitat*. Proceedings of Theme B, Volume 1, XXVII IAHR Congress, 10–15 August, San Francisco, Holly FM, Alsaffar A (eds). ASCE: New York, 1997; 45–50.
6. Addison PS, Qu B, Nisbet A, Pender G. A non-Fickian, particle-tracking diffusion model based on fractional Brownian motion. *International Journal for Numerical Methods in Fluids* 1997; **25**: 1373–1384.
7. Addison PS, Qu B, Ndumu AS, Pyrah IC. A particle-tracking model for non-Fickian subsurface diffusion. *Mathematics in Geology* 1998; **30**(6): 695–716.
8. Addison PS. *Fractals and Chaos: An Illustrated Course*. Institute of Physics Publishing: Bristol, 1997.
9. Mandelbrot BB, Van Ness JW. Fractional Brownian motions, fractional noises and applications. *SIAM Review* 1968; **10**: 422–437.
10. Mandelbrot BB, Wallis JR. Computer experiments with fractional Gaussian noises. Part 3, mathematical appendix. *Water Resources and Research* 1969; **5**: 260–267.
11. Mandelbrot BB. *The Fractal Geometry of Nature*. WH Freeman and Company: New York, 1983.
12. Hurst HE. Long term storage capacity of reservoirs. *Transactions of the ASCE* 1951; **116**: 770–808.
13. Mandelbrot BB. A fast fractional Gaussian noise generator. *Water Resources and Research* 1971; **7**: 543–553.
14. Rambaldi S, Pinazza O. An accurate fractional Brownian motion generator. *Physica A* 1994; **208**: 21–30.
15. Peitgen H-O, Saupe D. *The Science of Fractal Images*. Springer: New York, 1988.
16. Voss RF. Random fractals: Self–affinity in noise, music, mountains, and clouds. *Physica D* 1989; **38**: 362–371.
17. Yin Z-M. New methods for simulation of fractional Brownian motion. *Journal of Computational Physics* 1996; **127**: 66–72.
18. Hewett TA. Fractal distributions of reservior heterogeneity and their influence on fluid transport. Paper presented at the 61st Annual Conference and Exhibition, Society of Petroleum Engineers, SPE 15386, New Orleans, LA, 1986.
19. Hewett TA. Modelling reservior heterogeneity with Fractals. In *Geostatistics Trioa '92*, vol. 1, Soares A (ed.). Kluwer Acaddemic: Norwell, MA, 1992; 455–466.
20. Cooley JW, Lewis PAW, Welch PD. The fast Fourier transform and its applications. *IEEE Transactions on Education* 1969; **12**(1): 27–34.
21. Brigham EO. *The Fast Fourier Transform*. Prentice Hall: Englewood Cliffs, NJ, 1974.
22. Press WH, Teukolsky SA, Vetterling WT, Flannery BP. *Numerical Recipes in Fortran: The Art of Scientific Computing*. Cambridge University Press: New York, 1992.
23. Shinozuka M, Jan C-M. Digital simulation of random processes and its application. *Journal of Sound and Vibration* 1972; **25**(1): 111–128.
24. Foister RY, Van Den Ven TGM. Diffusion of Brownian particles in shear flows. *Journal of Fluid Mechanics* 1980; **96**(1): 105–132.
25. Addison PS, Bo Q, Ndumu AS, Mead CT. Non-Fickian dispersion in coastal waters. In *13th ASCE Engineering Mechanics Division Conference*. Baltimore, MD, 13–16 June, 1999.
26. Osborne AR, Kirwan AD, Provenzale A, Bergamasco L. Fractal drifter trajectories in the Kuroshio Extension. *Tellus* 1989; **41A**: 416–435.

27. Sanderson BG, Goulding A, Okubo A. The fractal dimension of relative Lagrangian motion. *Tellus* 1990; **42A**: 550–556.
28. Sanderson BG, Booth DA. The fractal dimension of drifter trajectories and estimates of horizontal eddy-diffusivity. *Tellus* 1991; **43A**: 334–349.
29. Wang KG, Lung CW. Long-time correlation effects and fractal Brownian motion. *Physics Letters A* 1990; **151**(3/4): 119–121.
30. Addison PS, Ndumu AS. Engineering applications of fractional Brownian motion: self-similar and self-affine random processes. *Fractals* 1999; **7**(2): 151–157.
31. Addison PS, McKenzie WMC, Ndumu AS, Dougan L, Hunter R. Fractal cracking of concrete: parameterisation of spatial diffusion. *ASCE Journal of Engineering and Mechanics* 1999; **125**(6): 622–629.
32. Addison PS. Towards a non-Fickian diffusion model using fractal geometric techniques. *ASCE Journal of Hydraulic Engineering* 1998; **124**(9): 877–879.
33. Johnson WB, Ludwig FL, Dabberdt WF, Allen RJ. An urban diffusion simulation model for carbon monoxide. *Journal of the Air Pollution Control Association* 1973; **23**(6): 490–498.
34. Yamartino RJ, Wiegand G. Development and evaluation of simple models for the flow, turbulence and pollutant concentration fields within an urban street canyon. *Atmospheric Environment* 1986; **20**(11): 2137–2156.
35. Lanzani G, Tamponi M. A microscale Lagrangian particle model for the dispersion of primary pollutants in a street canyon. *Atmospheric Environment* 1995; **29**: 3465–3475.
36. Addison PS, McCann JM, Low DJ, Currie JI. An integrated approach to modelling traffic pollution in the urban environment. *Traffic Engineering and Control* 1999; **September**: 434–439.
37. Qu B. The use of fractional Brownian motion in the modelling of dispersion of contaminants in fluids. PhD thesis, Napier University, Edinburgh, UK, 1999.

